A parametric study of process design and cycle configurations for pre-combustion PSA applied to NGCC power plants

Azpiri, Rebeca; Wood, Joe

DOI:
10.1016/j.cherd.2020.04.039

Document Version
Peer reviewed version

Citation for published version (Harvard):
Azpiri, R & Wood, J 2020, 'A parametric study of process design and cycle configurations for pre-combustion PSA applied to NGCC power plants', *Chemical Engineering Research and Design*, vol. 160, pp. 141-153. https://doi.org/10.1016/j.cherd.2020.04.039

A parametric study of process design and cycle configurations for pre-combustion PSA applied to NGCC power plants

*Rebeca A. Azpiri Solares, Joseph Wood**

School of Chemical Engineering, University of Birmingham, Edgbaston, Birmingham B15 2TT, United Kingdom

*Corresponding author. E-mail address: J.Wood@bham.ac.uk.

ABSTRACT: Natural gas combined cycle (NGCC) power plants show favorable conditions for the implementation of pressure swing adsorption (PSA) for the capture of carbon dioxide. These plants also show the advantage of a hydrogen co-production system. The challenge when implementing PSA in these plants is to achieve reference configurations that can obtain both products (hydrogen and carbon dioxide) at high purity levels, maximizing the recovery of hydrogen as a valuable product. This study presents the scale-up of a previously reported laboratory-based, four-bed, seven-step PSA model and a parametric study of the scaled-up PSA variables to maximize the product performance parameters. The capacity of the PSA model is based on the flow rate requirements of a GE-10 gas turbine, which can operate with up to 95% hydrogen purity. A parametric study using global system analysis (GSA) showed the effect of the bed diameter, length-to-diameter ratio and purge-to-feed flow rate ratio upon the product performance parameters. A purity of carbon dioxide of 95.37% and a hydrogen recovery of 92.27% was obtained with a purge-to-feed flow rate ratio of 0.22. The purity of hydrogen

stayed close to 99.99%, with maximum deviations around 0.0001% for all case studies. The purity of the carbon dioxide and the recovery of hydrogen were further improved by considering additional PSA configurations. The addition of an assisted purge step and three pressure equalization steps improved these performance parameters by two percentage points. Overall, the model with one pressure equalization step, assisted purge step and rinse step after the feed step showed promising results with a purity of carbon dioxide of 98.28% and hydrogen recovery of 95.48%. Lower capitals costs are expected for this configuration, compared to adding pressure equalization steps using more than four fixed-bed units.

KEYWORDS: CCS, NGCC, PSA, Parametric study, Process simulation

Nomenclature

C_i	Concentration of the i component in the gas phase, mol/m^3
Q_i	Sorbent loading of the i component, mol/kg
$\boldsymbol{\rho}$	Gas density, kg/m^3
$\boldsymbol{\rho_s}$	Particle density, kg/m^3
$\mathcal{E}_b$	Bed void fraction
$\mathcal{E}_p$	Particle void fraction
$\mathcal{E}_t$	Total void fraction
v	Gas velocity, m/s
R	Ideal gas constant, J/(mol K)
t	Time, s
T	Temperature, K
T_w	Wall temperature, K
P	Pressure, bar

λ	Heat axial dispersion coefficient, J/(s m K)
ΔH_i^{ads}	Heat of adsorption of the i component, J/mol
C^i_{pg}	Specific heat of the i component in the gas phase, J/(mol K)
C_{ps}	Sorbent specific heat, J/(kg K)
h_i	Effective heat transfer coefficient, J/(m^3 s K)
μ_g	Viscosity of the gas phase, (Pa s)
D_p	Sorbent particle diameter, m
b_i	Langmuir equilibrium constant of the i component, 1/Pa
K_i	Effective mass transfer coefficient of the i component, 1/s
q_{mi}	Maximum sorbent loading of the i component, mol/kg
D_{AB}	Diffusion coefficient, m^2/s
D_x	Mass axial dispersion coefficient, m^2/s
L	Bed length, m
F_i	Molar flow rate of i component, mol/s
Q_n	Normalized volumetric flow rate, m^3/s
A_{bed}	Fixed-bed reactor area, m^2
i=1…n	Number of components

List of abbreviations

L/D	Fixed-bed length-to-diameter ratio
Pu/F	Purge-to-feed flow rate ratio
P	Pressurization step
A	Adsorption step
D	Depressurization step
PE-D	Pressure equalization-depressurization step
PE-P	Pressure equalization-pressurization step
A-Pu	Assisted purge step
R	Rinse step

Pu	Purge step

1. Introduction

Climate change caused by global carbon dioxide emissions is regarded as one of the main challenges that the world will face in the next 50 years. Carbon capture and storage (CCS) is a technology able to decarbonize energy supplies that would otherwise generate carbon emissions (Heuberger et al., 2017; Mac Dowell and Staffell, 2016). In fact, the implementation of the technology worldwide will be critical if fossil fuel reserves are still substantially in use by 2050 and an increase of no more than 2°C in the global temperature is to be met (Budinis et al., 2018). Additionally, a system with purely renewable energy needs the implementation of an effective energy storage network; this is still not ready for implementation (Heuberger et al., 2017).

The IPCC indicated in 2005 that a number of CCS technologies were ready for bench scale demonstration, because large gas separation processes were operating in industry (Abanades et al., 2015). The main technologies of carbon capture implemented at large scale involve chemical absorption in post-combustion conditions applied to coal fired power plants, such as the Petra nova CCS project. This plant captures about 90% carbon dioxide of the flue gas coming from a 240MW combustion facility (U.S. Energy Information Administration, 2017). The energy penalty of a pulverized coal fired power plant using post-combustion carbon capture has been reported to be between 15 and 28% (Budinis et al., 2018).

Integrated gasification and natural gas combined cycle (IGCC and NGCC) power plants demonstrate a high potential to adopt CCS technologies and to reduce capture costs, as the

energy penalty for these plants is expected to be between 4.9 and 20% (Budinis et al., 2018). This is due to carbon dioxide concentrations as high as 30 to 40% in the flue gas and high gas pressures between 20 and 40 bar that reduce compression requirements before combustion (Agarwal et al., 2010; Ju and Lee, 2017; Lee et al., 2014; Lee et al., 2014). Specifically, pre-combustion CCS applied to NGCC power plants could show advantages with regards to the operating cost of the plant and degree of success of the purification process, due to the composition of the natural gas compared to the one in coal.

Pre-combustion power plants have been implemented at a large scale using solvent based absorption, such as the ELCOGAS 335MW IGCC plant in Puertollano (Rackley, 2017). These power plants could also offer the advantage of implementing a hybrid power-hydrogen production system (Riboldi and Bolland, 2016; Seyitoglu et al., 2016). In fact, CCS is regarded as one of the main technologies for future hydrogen production (Grande, 2012). Hydrogen is regarded as one of the main energy vectors in a zero-emissions future, to decarbonize a number of sectors, such as industrial heat and transport. The production of hydrogen is currently responsible of around 700 mtpa (million tonnes per annum) of carbon dioxide emissions, according to the IEA (Gasworld, 2019).

Pressure Swing Adsorption (PSA) has been considered the potential capture technology to be adopted in IGCC and NGCC power plants, due to the high energy efficiency of the industrial gas separation process (Abanades et al., 2015; Jansen et al., 2015; Moon et al., 2018; Riboldi and Bolland, 2015a). The capacity of the industrial plant, the final purity and recovery of the products, and the rate of energy consumption of the process dictate the arrangement of the PSA process steps and the number of fixed-bed adsorber units. A H_2 rich syngas would be produced from the process and provided to a gas turbine for power generation (Lee et al., 2017). This is a next generation technology where gas turbines operating with over 95% hydrogen gas streams

are ready for implementation (Cappelletti and Martelli, 2017; Goldmeer, 2018). In this context, hydrogen fueled turbine efficiency and temperature issues are regarded as the main barrier for the implementation of pre-combustion capture (Rackley, 2017).

Industrial PSA processes aim to obtain high recovery and purity of the light product, such as the production of hydrogen from natural gas (Ribeiro et al., 2008).The challenge of the process when implemented for CCS is also to obtain a high purity of the heavy product, carbon dioxide. For this purpose, there is no simple accepted process configuration that effectively concentrates the carbon dioxide. Consequently, there is a need to arrive at reference process configurations; mathematical simulation is used as a tool to predict these (Abanades et al., 2015).

On the one hand, most of the work done in PSA configuration and optimization studies has applied to hydrogen purification processes from natural gas feed containing CO_2, CO, CH_4, N_2 and H_2 (Cavenati et al., 2006; Luberti et al., 2014; Moon et al., 2016; Nikolic et al., 2008; Ribeiro et al., 2008). These studies obtained hydrogen that was up to 99% pure. They suggested that multiple adsorbent layers would be convenient for improving the hydrogen recovery and purity when using multiple beds in the system, due to the number of components that enter the separation unit. These previous studies did not analyze the arrangement of steps that would also give high purity of the heavy product.

On the other hand, there are some studies that analyzed the arrangement of the PSA steps in IGCC power plants that would optimize the recovery and the purity of the carbon dioxide (Agarwal et al., 2010; Wang et al., 2015). One of the novelties of these studies was recycling the carbon dioxide product to the feed during the depressurization step. The purity of the resulting carbon dioxide was over 90%. However, the studies were limited to the interaction

between two beds and did not show the effect that multiple pressure equalization steps between beds or a carbon dioxide rinse step would have on the gas product.

Another recent study analyzed the effect of a number of parameters for a four-bed and eight-bed pressure swing adsorption process on the final recovery and purity of hydrogen in IGCC power plants (Moon et al., 2018). Pressure equalization was used to reduce the amount of tail gas (heavy product) in the hydrogen. Recycled hydrogen was used as a purging gas to increase the product recovery to 99%. However, the study did not show the process arrangement that would give over 95% carbon dioxide purity, which is the requirement for carbon dioxide storage and utilization (Abanades et al., 2015; Webley, 2014).

The aim of this study was to analyze a number of PSA process configurations to obtain over 95% purity in both hydrogen and carbon dioxide products and recover over 90% of the hydrogen, with the process conditions of a NGCC power plant. The authors previously reported a laboratory scale PSA model, with parameter estimation and validation based on laboratory measurements of adsorption isotherms and breakthrough curves using amine modified activated carbon adsorbents (Azpiri Solares et al., 2019).

This study analyzes the process design of scaling-up the validated model to treat 293 mol s^{-1} of a hydrogen and carbon dioxide gas mixture, 60% and 40% (mol basis), respectively, at a pressure of 36.7 bar and 338 K defined from the process up-stream. Then, in a parametric study, the purity of the products was improved by varying the scaled-up process variables; diameter and length of the bed and the feed-to-purge flow rate ratio. The aim of this analysis was to study the effect of the scaled-up design on the PSA performance parameters (recovery and purity of the products).

120 Additionally, as it is challenging to establish an optimization framework by varying a
121 number of fixed-bed reactors, four-, five- and six-bed PSA models were developed such that
122 each model included a number of process configurations. The aim of analyzing the number of
123 units and steps of the process was to establish a framework to see which PSA configurations
124 could be suitable for the gas products specifications in a NGCC power plant.

125 Previous studies have reported the effect of one to four pressure equalization steps and
126 providing purge step on the purity and recovery of the product, for the synthesis of hydrogen
127 and natural gas upgrading (Grande et al., 2017; Jiang et al., 2004; Luberti et al., 2014; Moon
128 et al., 2018; Ribeiro et al., 2008). This study analyzes the effect of these steps and adds a longer
129 rinse step than a purge step at 1 bar to obtain carbon dioxide purity requirements for storage
130 and utilization applied to NGCC power plants.

131

132 **2. Design**

133 *2.1. The PSA model and scale up approach*

134 The authors previously reported a laboratory scale fixed-bed reactor model (Azpiri Solares
135 et al., 2019), and the purpose of this article is to report its scale-up using a number of cycle
136 designs and based on 293.2 mol s^{-1} gas fed into the PSA system. The aim of scaling up the PSA
137 model was to analyze the effect of the design and process variables on the product performance
138 parameters at plant scale.

139 The previously reported experimental adsorption process was validated against a one-
140 dimensional dispersed plug-flow model that made the following assumptions: (i) the gas
141 flowing through the reactor is considered ideal, (ii) there are no radial variations in the pressure,
142 temperature and concentration of the overall gas and the components, (iii) there is thermal

equilibrium between the gas and the solid phase, (iv) the solid bulk density remains constant, and (v) the limiting step of the mass transfer between the gas and the solid phase is the diffusion of the components through the micro-pores, described by the previously validated Linear Driving Force (LDF) model (Moon et al., 2018; Ribeiro et al., 2008).

The overall and component mass balances and the non-isothermal energy balance were calculated based on these previous assumptions. The Langmuir isotherm, Eq (4), successfully predicted the carbon dioxide adsorption equilibrium data, and the Ergun equation, Eq (5), was used to describe the pressure drop in the fixed-bed reactor (Azpiri Solares et al., 2019). Eqs (1)–(7) show the ordinary and partial differential equations used in the model.

$$\varepsilon_t \frac{\partial C(z)}{\partial t} = -\varepsilon_b \frac{\partial (C(z)v(z))}{\partial z} + \varepsilon_b D_x \frac{\partial^2 C(z)}{\partial z^2} - (1-\varepsilon_b)\rho_s \sum_{i=1}^{N_{comp}} \frac{\partial Q(i,z)}{\partial t} \quad (1)$$

$$\varepsilon_t \frac{\partial Y(i,z)}{\partial t} = -\varepsilon_b v(z) \frac{\partial Y(i,z)}{\partial z} + \varepsilon_b D_x \left(\frac{\partial^2 Y(i,z)}{\partial z^2} + \frac{2}{C(z)} \frac{\partial Y(i,z)}{\partial z} \frac{\partial C(z)}{\partial z}\right) - \frac{(1-\varepsilon_b)\rho_s}{C(z)} \left(\frac{\partial Q(i,z)}{\partial t} - Y_{(i,z)} \sum_{i=1}^{N_{comp}} \frac{\partial Q(i,z)}{\partial t}\right) \quad (2)$$

$$\rho c_{p,g(z)} \frac{\partial (T(z)v(z))}{\partial z} + \varepsilon_t \rho c_{p,g(z)} \frac{\partial T(z)}{\partial t} + \varepsilon_t \rho_s c_{p,s} \frac{\partial T(z)}{\partial t} - (1-\varepsilon_b)\rho_s \sum_{i=1}^{N_{comp}} \Delta H_{ads(i)} \frac{\partial Q_{(i,z)}}{\partial t} + h_i (T(z) - T_{wall}) = \lambda \frac{\partial^2 T(z)}{\partial z^2} \quad (3)$$

$$Q^*_{(z)} = \frac{q_{mi} b_i P(z) RT(z)}{1 + b_i P(z) RT(z)} \quad (4)$$

$$-\frac{\partial P(z)}{\partial Z} = 150\, u_{g(z)} \frac{(1-\varepsilon_b)^2}{D_p^2 \varepsilon_b^3} v(z) + 1.75 \frac{(1-\varepsilon_b)\rho}{D_p \varepsilon_b^3} v(z)|v(z)| \quad (5)$$

$$\frac{\partial Q_{(i,z)}}{\partial t} = K_{(i)} (Q^*_{(i,z)} - Q_{(i,z)}) \quad (6)$$

$$C(z) = \frac{P(z)}{R\, T(z)} \quad (7)$$

163

164 The basic case study for this model considered four fixed-bed reactors operating
165 simultaneously. This is the minimum number of beds required in a NGCC power plants for a
166 pressure swing adsorption cycle, as there is a minimum of four steps in a PSA cycle and there
167 must be continuous production of hydrogen. These number of beds are required for the
168 continuous feed of hydrogen to the gas turbine during depressurization and pressurization steps
169 for a base four-step Skarstrom cycle (Ruthven et al., 1994). If fewer than four beds were
170 implemented, hydrogen storage would be required; this would be challenging in terms of cost
171 and safety. The boundary conditions of the PSA model are shown in Eqs (8)-(14).

172

173 $$-\varepsilon_b D_x \frac{\partial C_i}{\partial z}_{z=0} = v_{z=0}(C_{i,feed} - C_{i,z=0}) \quad (8)$$

174 $$-\varepsilon_b \lambda \frac{\partial T}{\partial z}_{z=0} = v_{z=0}\rho c_{p,g,z=0}(T_{feed} - T_{z=0}) \quad (9)$$

175 $$v_{z=0} = v_{feed} \quad (10)$$

176 $$\frac{\partial C_i}{\partial z}_{z=L} = 0 \quad (11)$$

177 $$\frac{\partial T}{\partial z}_{z=L} = 0 \quad (12)$$

178 $$\frac{\partial v}{\partial z}_{z=L} = 0 \quad (13)$$

179 $$P_{z=L} = P_{end} \quad (14)$$

180

181 The outlet boundary condition of the pressure during the depressurization, pressurization
182 and pressure equalization steps was described by a transition equation between the adsorption

pressure (P_{ads}), equalization pressure (P_{eq}), and the atmospheric pressure (P_{atm}). The change was described by a first order differential equation that modelled a linear valve, shown in Eqs (15)-(16).

$$\frac{\partial P_{depress}}{\partial t}_{z=L} = -\left(\frac{P_{ads/eq} - P_{atm}}{t_{depressurization}}\right) \quad (15)$$

$$\frac{\partial P_{press}}{\partial t}_{z=L} = \left(\frac{P_{ads/eq} - P_{atm}}{t_{pressurization}}\right) \quad (16)$$

The following steps were considered for the base study: (i) an adsorption step at 36.7 bar, A, with 40% CO_2 and 60% H_2 molar fractions; (ii) a depressurization-pressure equalization step, PE-D, in which the outlet stream of the depressurizing bed is connected to a pressurizing bed, until the depressurizing bed reaches 5 bar; (iii) a total depressurization step until 1 bar, D, where the outlet gas goes to the carbon dioxide product; (iv) a rinse step, R, at 1 bar and with a 100% CO_2 feed molar fraction coming from a carbon dioxide storage tank; (v) a purge step, Pu, with a 100% H_2 feed molar fraction coming from the adsorption step; (vi) a pressurization-pressure equalization step, PE-P, with the same duration of the pressure equalization step during the depressurization; and (vii) a total feed pressurization step until 36.7 bar, P. The depressurization and pressurization of the bed were set to a rate that matched the adsorption time, for the sake of synchronizing the beds. The rinse and purge durations were of 5/6 and 1/6 of the adsorption step, respectively, to return the bed to a clean stage. The schematic representation of this process is shown in Figure 1.

Figure 1.

In order to simulate the four-bed model, a uni-bed model was assumed for the multi-bed PSA simulations. This was done by storing the results of the outlet gas (concentration, pressure and temperature) during the depressurization-pressure equalization process and entering this data in the same step during the pressurization process, because these steps are the only steps when two beds interact. This approach is supported by previous PSA studies and reduces the amount of computational time (Casas et al., 2013; Ribeiro et al., 2008; Riboldi et al., 2014).

The scale up of the PSA model was based on a 293.2 mol s^{-1} feed into the PSA process from upstream. These data derive from the hydrogen flow rate needs of a GE-10 gas turbine, which can operate with over 95% hydrogen purity (Goldmeer, 2018). The flow rate fed into the gas turbine determines the sizing and the conditions of the PSA process, together with the operating feed composition, pressure and temperature from the process upstream of the PSA unit. The normalized flow rate (Nm^3 s^{-1}) was derived using the ideal gas equation, Eq (7), and included the feed pressure and temperature (these values are also set by the process up-stream). The feed conditions from the process upstream were established from the outlet stream of the water gas shift reactor described by the European Bench Marking Task Force (2011), with a value of 36.7 bar and 523 K. The water gas shift outlet gas temperature would be decreased to 338 K to enter the PSA unit as reported in a previous study (Riboldi and Bolland, 2015b).

The volumetric flow rate at a feed pressure of 36.7 bar was 0.2 m^3 s^{-1}. The adsorption time was established to 300 s, based on the feed pressure and the breakthrough capacity of the adsorbent (Jain et al., 2003). The superficial velocity of a pilot-scale or industrial fixed-bed reactor is typically between 0.01 and 0.05 m/s, which is a compromise between the productivity of the unit and avoiding fluidization inside the reactor (Wiheeb et al., 2016). With a superficial velocity of 0.04 m s^{-1}, the diameter of the reactor was 2.57 m.

The length of the reactor was determined using a length to diameter ratio (L/D) of 1.51, based on the amount of carbon dioxide moles to treat during the fixed adsorption time and to show the breakthrough time of the carbon dioxide at 600 s when the depressurization step reaches 1 bar, as well as, previous PSA studies (Riboldi and Bolland, 2015b). The wall thickness of the fixed-bed reactor should be between 1 mm and 10 mm and it was used to calculate the heat transfer through the walls (Rase, 1990). For this system, 7×10^{-3} m was chosen, due to severe pressure inside the fixed-bed reactor in the adsorption step. The particle diameter was 1×10^{-3} m (the same as laboratory scale). Table 1 shows the rest of the parameters of the adsorbent and of the reactor used in this case study of the PSA model. For this process, the parameters of a previously reported Activated Carbon Norit® RB1 adsorbent modified with MEA-MDEA (1:0.6, mol AC:mol MEA-MDEA) were used in the simulation (Azpiri Solares et al., 2019). The isotherm parameters and mass transfer coefficient of the carbon dioxide towards the activated carbon were calculated from the laboratory data and parameter estimation of the previous work, respectively. The mass transfer coefficient of the hydrogen, as well as, the axial mass and heat dispersion coefficients were calculated using the Wakao and Funazkri (1978) correlation. The isotherm parameters of hydrogen are the ones reported by Riboldi et al. (2014) for the activated carbon.

Table 1. Fixed-bed reactor and adsorbent parameters for the PSA simulation.

Adsorbent and fixed-bed reactor data			
Particle density, ρ_s (kg m^{-3})	262	Bed diameter, D (m)	2.57
Particle void fraction, ε_p	0.74	Bed void fraction, ε_b	0.48
Particle diameter, d_p (m)	0.001	Bed length, L (m)	3.88
Effective heat transfer coefficient, h_i (kW m^{-2} K^{-1})	500	Wall specific heat, cp_w (kJ kg^{-1} K^{-1})	0.46

Effective mass transfer coefficient, K_i (s^{-1})	CO_2: 0.046 H_2: 0.092	Wall thickness, L_w (m)	0.007
Axial mass dispersion coefficient, D_x ($m^2 s^{-1}$)	9.3×10^{-5}	Wall density, ρ_w ($kg\ m^{-3}$)	7700
Axial heat dispersion coefficient, λ ($W\ m^{-1}\ K^{-1}$)	1.5		
Maximum monolayer coverage capacity for CO_2, $q_{m,CO2}$ ($mol\ kg^{-1}$)	9.2	Langmuir equilibrium constant for CO_2, b_{CO2} (Pa^{-1})	3×10^{-6}
Maximum monolayer coverage capacity for H_2, $q_{m,H2}$ ($mol\ kg^{-1}$)	23.57	Langmuir equilibrium constant for H_2, b_{H2} (Pa^{-1})	7.69×10^{-11}

2.2. Design variations in the PSA cycle

The choice of several process variables when scaling up the PSA process has an effect on the separation process and, thus, on the composition of the outlet streams in each of the process steps shown in Figure 1. The capacity of a NGCC plant is determined as the number of moles of hydrogen gas required to produce a certain power; this logically also determines the number of moles that must enter the PSA separation process that was established with a constant value of 293.2 mol s^{-1}, at 36.7 bar and 338 K from the process upstream, a water gas shift reactor (WGS) and a cooler.

Once the feed molar flow rate, pressure and temperature were established, the main operational variables were the superficial velocity of the gas ($v_{(0)}$) dependent of the bed diameter, the length-to-diameter ratio of the bed (L/D) and the purge-to-feed flow rate ratio (Pu/F). Figure 2 shows the flow diagram for the various design choices of the PSA process explained here.

Figure 2.

The effect of the PSA decision variables was analyzed using the Global System Analysis (GSA) capability in gPROMS® ProcessBuilder 1.3.1. This capability enables users to explore the behavior of the system, based on a set of input variables. A number of model simulations are simultaneously performed for a selected range of the decision variables. A parametric study was executed by inserting a range of the input values shown in Figure 2 and obtaining the purity values of hydrogen and carbon dioxide, with a requirement of achieving over 85% recovery of hydrogen in each of the case studies. The range of the parameters for this study were chosen based on the previous conditions given for PSA studies that separate hydrogen and carbon dioxide.

The partial differential equations (PDEs) for each of the parametric studies were solved using the forward finite difference method (FFDM) and the backward finite difference method (BFDM), depending on the direction of the flow. Grid independence for the discretization scheme was achieved by varying the discretization points from 50 to 100. Initially, it was assumed that the bed was filled with 100% pure hydrogen at feed pressure and ambient temperature, in order to initialize the partial differential equations. The performance indicators of this parametric study, the purity of carbon dioxide and hydrogen, were calculated using Eqs (17)–(18), and the recovery of the products was calculated using Eqs (19)–(20).

$$CO_2\ Purity = \frac{\int_{t=t_D}^{t=t_{Pu}} C_{CO_2,z=L} v_{z=L} dt}{\sum_{i=1}^{n} \int_{t=t_D}^{t=t_{Pu}} C_{i_{z=L}} v_{z=L} dt} \quad (17)$$

$$H_2\ Purity = \frac{\int_{t=0}^{t=t_A} C_{H_2,z=L} v_{z=L} dt}{\sum_{i=1}^{n} \int_{t=0}^{t=t_A} C_{i_{z=L}} v_{z=L} dt} \quad (18)$$

$$H_2\ Recovery\ =\ \frac{\int_{t=0}^{t=t_A} C_{H_2,z=L} v_{z=L} dt - \int_{t=t_R}^{t=t_{Pu}} C_{H_2,z=0} v_{z=0} dt}{\int_{t=0}^{t=t_A} C_{H_2,z=0} v_{z=0} dt + \int_{t=t_{Pu}}^{t=t_P} C_{H_2,z=0} v_{z=0} dt} \quad (19)$$

$$CO_2\ Recovery\ =\ \frac{\int_{t=D}^{t=t_{Pu}} C_{CO_2,z=L} v_{z=L} dt}{\int_{t=0}^{t=t_A} C_{CO_2,z=0} v_{z=0} dt + \int_{t=t_{Pu}}^{t=t_P} C_{CO_2,z=0} v_{z=0} dt} \quad (20)$$

3. Additional beds and configurations

Once the operational conditions and design parameters were established using the parametric study results, additional configurations and beds were included in the model. The number of beds is one of the variables that dictate the number and types of steps in a PSA model. The goal of the alternative configurations was to raise the carbon dioxide purity, because the target of 99% purity of the hydrogen was obtained with the previous case studies using GSA. Additional configurations were based on the four-bed base case, adding one (a five-bed model) and two (a six-bed model) reactors. Cases beyond a six-bed PSA model have not been studied here, as more beds would critically raise the capital costs (CAPEX) of a NGCC power plant (Casas et al., 2013).

Additional configurations for the four-bed model were investigated: introducing an assisted purge step (A-Pu) instead of the depressurization step. The assisted purge step used the outlet gas of the depressurizing bed until 1 bar, as the feed gas during the purge step. The effect of including a rinse step (R1), feeding carbon dioxide after the adsorption and pressure equalization steps, was also studied. The durations of the assisted purge step and the rinse step were the same (50 s) in order to synchronize the beds.

The effect of introducing an assisted purge step and a rinse step was also tested on the five- and six-bed models. These models offered the introduction of additional pressure equalization steps; the five-bed model had two pressure equalization steps and the six-bed model had three

pressure equalization steps. It has been previously reported that the addition of pressure equalization steps increases the carbon dioxide purity and the hydrogen recovery (Casas et al., 2013). The insertion of additional pressure equalization steps also allows the process to include the rinse step between the first and second pressure equalization steps (in the five-bed model) and the second and third equalization steps (in the six-bed model). This last step decreases the compression requirements compared to a rinse step after the feed step at adsorption pressure of 36.7 bar, for the gas product coming from the assisted purge step at 1 bar.

4. Results and discussion

4.1. Comparison between the laboratory based and scaled-up PSA model

Firstly, the performance parameters of recovery and purity, calculated using Eqs (17)–(20), and the evolution of the product mole fractions at the outlet of the bed were compared for the laboratory and the scaled-up PSA models. The PSA cycle used for this comparison is shown in Figure 1, which adds a carbon dioxide rinse step followed by a purge step to previously reported PSA cycles (Moon et al., 2018; Ribeiro et al., 2008). Both simulations were performed until Cyclic Steady State (CSS) was achieved, where the drop of the product performance parameters was of the order of 0.0005% in the case of purity, and 0.008% in the case of recovery. CSS was achieved after 497 cycles in both of the case studies, when the temperature profiles were stable in the gas phase for 10 consecutive cycles.

On the one hand, the PSA configuration shown in Figure 1 follows previous depressurization and pressurization steps commonly reported in the literature, since the inclusion of a pressure equalization step was regarded as necessary to improve the recovery of hydrogen (Moon et al., 2018). On the other hand, a rinse step with carbon dioxide at 1 bar was necessarily added to the cycle to increase the purity of carbon dioxide. This step has not

commonly been implemented in previous PSA studies because carbon dioxide has not been the product of interest. The duration of the purge step with hydrogen at 1 bar was set to be 1/5 of that for the rinse step, in order to purge the remaining carbon dioxide gas out of the bed and to maximize the hydrogen recovery.

Figure 3a and Figure 3b show the molar hydrogen and carbon dioxide component fractions at the outlet of the bed for the laboratory and scaled-up PSA cycle, respectively. Both of models follow the configuration shown in Figure 1. During the adsorption time (300 s), hydrogen gas that was around 99.99% pure came out of the bed and the carbon dioxide remained adsorbed in the activated carbon inside the bed at 36.7 bar. The depressurization-pressure equalization step lasted for 250 s (up to 5 bar) and carbon dioxide remained adsorbed in the bed until the end of this step. The 99.99% pure hydrogen stream coming from the depressurization-pressure equalization bed was used to pressurize another bed.

Figure 3a.

Figure 3b.

The carbon dioxide product was obtained as soon as the depressurization step started and during the rinse (250 s) and purge steps (50 s). It took the last seconds of the depressurization step and the initial seconds of the rinse step to reach around 99.99% pure carbon dioxide exiting the bed and purity remained at that level until the rinse step finished for both PSA processes.

There was a slight difference between the laboratory and the scaled-up process when the hydrogen purge was fed at 1 bar to the system: the carbon dioxide concentration decreased rapidly during those 50 s in the laboratory process to 43% purity, but decreased to 84% purity

for the scaled-up process. The slower decrease of the carbon dioxide concentration during the scaled-up process can be explained by the greater length of the reactor and the longer residence time: the response to a component entering the system occurs later.

The purity of hydrogen obtained for both of the processes was 99.99%. The purity of carbon dioxide was 84.7% in the laboratory set-up and 86.4% in the scale up process. Hydrogen recovery was 87.6 % in both systems, and the recovery of carbon dioxide was lower than 85%.

The temperature evolution in the fixed-bed reactor for both of the case studies was accounted using the energy balance shown in Eq (3). Figure 4 shows the temperature profile for the four-bed scaled-up model, where there is a temperature variation of 15°C before the depressurization step starts. This rise of temperature happens during the adsorption step at the end of the bed, and then is compensated by the desorption, purge and rinse steps. The temperature variation is in the range of previous studies using activated carbon adsorbents at high pressures in fixed-bed reactor units (Ribeiro et al., 2008).

Figure 4.

4.2. Parametric study of the scaled-up PSA process variables

4.2.1. Effect of the superficial gas velocity varying the bed diameter

The effect of the superficial gas velocity was investigated in the process shown in Figure 1. For this purpose, the superficial gas velocity was varied by changing the bed diameter at a constant molar flow rate of 293.2 mol s^{-1} and pressure of 36.7 bar, following the steps given in Figure 2. The length of the bed was constant and was set at the value of the basic case study

shown previously (3.88 m). Therefore, as the bed diameter was an experimental variable in this study, different bed length to diameter (L/D) ratios were used for each of the studied case.

The parametric study simulated by the Global Systems Analysis (GSA) studied the effect of the superficial velocity and diameter of the reactor on the product performance parameters. A quasi-random sampling method was applied that executed the analysis by distributing the variable values uniformly across the sampling range selected. The sampling range selected for the superficial velocity was between 0.02 m s^{-1} (lower bound) and 0.05 m s^{-1} (upper bound). This sampling space was selected to avoid pressure drop and fluidization issues inside the fixed-bed reactor.

Figure 5 shows the results for the GSA using the superficial gas velocity as the decision variable. The figure relates the value of the decision variable to the purity of the carbon dioxide product. For all of the cases the purity of hydrogen stayed over 99.99%. These purity values were obtained with the process steps shown in Figure 1. The hydrogen was obtained during the adsorption step, which lasted for 300 s. This adsorption time was established as a compromise to maximize the purity of the hydrogen and to guarantee the cyclic recovery of the activated carbon based on the dynamic capacity of the material tested at laboratory scale. The carbon dioxide was obtained after the pressure equalization step, during the depressurization step (from 5 bar to 1 bar) and during the rinse (250 s) and purge (50 s) steps (at 1 bar).

Figure 5.

The hydrogen purity was not sensitive to the superficial velocity of the gas, nor to varying the diameter of the bed, which had a maximum variation of 0.0001% when operating at

superficial velocities between 0.02 m s^{-1} and 0.05 m s^{-1}. This insensitivity can be explained by the affinity of the carbon dioxide at 36.7 bar to the adsorbent surface compared to the affinity of the hydrogen for the range of superficial velocities chosen. Figure 5 shows that the carbon dioxide purity was more sensitive to the superficial velocity of the gas. The purity varied about 42% around the selected velocity values.

The purity of the carbon dioxide reached 92.93% when the superficial velocity was at the maximum limit of 0.048 m s^{-1}, as shown in Figure 5. In order to study this behavior, the concentration front of the carbon dioxide at the end of the bed during the PSA process was investigated for three runs in the sampling space of the GSA. Table 2 shows the values of the bed diameter for those runs. At a velocity of 0.048 m s^{-1}, the value of the bed diameter was 2.38 m, which is among the smallest diameter values for the sampling space selected. This result gives a higher length-to-diameter ratio of 1.63, compared to the result obtained with the basic case study, which had a bed diameter of 2.57 m.

Table 2. PSA product performance indicator values for three runs of GSA varying the superficial velocity (v).

Run	v (m s^{-1})	D (m)	Recovery H_2 (%)	Recovery CO_2 (%)	Purity H_2 (%)	Purity CO_2 (%)
1	0.036	2.75	87.56	83.57	99.999	57.54
2	0.039	2.64	86.45	83.72	99.999	77.51
3	0.048	2.38	84.56	84.13	99.994	92.93

The recovery of hydrogen varied about 2% over the three selected runs and 1% for the carbon dioxide product. The recovery of hydrogen decreased mainly due to the purge step and the inclusion of only one pressure equalization step in the four-bed PSA model. Run 3 yielded the lowest recovery value, 84.57%, due to the higher velocities mainly during the purge step.

4.2.2. Effect of the reactor length

The effect of the fixed-bed reactor length was studied by considering a number of length to diameter ratios at a constant diameter of 2.38 m, which gave the best performance in terms of overall product quality values, as explained previously. The length of the bed was discretized by the finite difference method in the PSA model. Therefore, the analysis could not be done via GSA, since the bed length needs to be a parameter with a fixed value for the discretization in the model but GSA requires a variable for the simulations using the Monte Carlo method. Instead, several runs varied the length to diameter ratio (L/D); then the trends of the component molar fractions at the end of the reactor and the product performance indicators were analyzed.

Table 3 shows the PSA performance parameter values for three runs that varied the length of the reactor and the corresponding length to diameter ratios for each of the runs. Figure 6 shows the carbon dioxide molar fractions in the outlet of the reactor from the adsorption until the purge step, where the carbon dioxide and hydrogen products were obtained. The best product purity values, taking both products into consideration, were obtained with a length to diameter ratio of 1.68, as shown in Table 3.

Figure 6.

Table 3. PSA product performance indicator values for the analysis that varied the bed length (L).

Run	L (m)	L/D	Recovery H_2 (%)	Recovery CO_2 (%)	Purity H_2 (%)	Purity CO_2 (%)

1	4	1.68	83.76	83.45	99.991	93.12
2	4.76	2	84.56	84.13	99.994	92.65
3	5.72	2.4	85.67	84.69	99.999	90.67

445

446 For the purity of the hydrogen, the three runs show a purity of 99.99%. Figure 6 shows that
447 with a length-to-diameter ratio of 1.68 (Run 1) and 2 (Run 2), the carbon dioxide started
448 desorbing at the end of the depressurization step (t = 600 s), which allowed to obtain carbon
449 dioxide purities as high as 93.12%. The slope of the desorbing carbon dioxide concentration
450 front was slower with a length-to-diameter ratio of 2.4, decreasing the carbon dioxide purity to
451 90.67%. The desorption rate is related to the pressure gradient in the reactor, thus the slower
452 desorbing rate of the carbon dioxide in a longer bed can be explained by the smaller pressure
453 gradient in the fixed-bed reactor compared to a shorter reactor.

454 The hydrogen and carbon dioxide recovery values decreased with smaller length to diameter
455 ratios, with a total decrease of 2% over all the simulations studied, but still did not achieve the
456 value of 90%, due to the amount of hydrogen used in the purge and rinse steps, as well as,
457 pressurization steps.

458

459 *4.2.3. Effect of the purge-to-feed flow rate ratio*

460 The effect of the purge-to-feed flow rate (Pu/F) was studied using GSA and following the
461 methodology explained for the superficial velocity. The purge flow rate was selected as a
462 varying parameter for the parametric analysis, which yielded a number of purge-to-feed ratios.
463 The purge flow rate was the flow rate at entry into the PSA reactor during the rinse and purge
464 steps. Afterwards, the flow rate was increased for the pressurization step until it reached the
465 adsorption flow rate. The range of purge-to-feed flow rate ratios selected was based on previous

PSA studies in which values ranged from 0.1 to 1 (Luberti et al., 2014; Moon et al., 2018; Ribeiro et al., 2008; Riboldi and Bolland, 2015a).

The carbon dioxide purity values from the GSA analysis are shown in Figure 7. The purity values of hydrogen were constant for this analysis, because hydrogen was obtained during the adsorption step and the only flow rate that varied during the analysis was the flow rate during the rinse and the purge steps. Figure 7 shows that the purity of carbon dioxide decreased with a linear trend with the increasing gas flow rate during the rinse and the purge steps. The PSA product performance parameters for three runs of the GSA sampling space are shown in Table 4.

Figure 7.

Of the three simulation runs, Run 1 gave the highest carbon dioxide purity. Although the flow rate of the carbon dioxide in the feed decreased during the rinse step, the overall purity of the carbon dioxide increased due to the smaller hydrogen flow rate during the 50 s purge.

Table 4. PSA product performance indicator values for three runs of the GSA while varying the purge-to-feed (Pu/F) flow rate ratio.

Run	Q_{Pu} (m^3 s^{-1})	Pu/F (-)	Recovery H_2 (%)	Recovery CO_2 (%)	Purity H_2 (%)	Purity CO_2 (%)
1	0.066	0.22	92.27	90.11	94.994	95.37
2	0.165	0.55	89.13	89.77	99.994	94.36
3	0.267	0.89	87.59	87.65	99.994	93.22

The decrease of the carbon dioxide feed flow rate during the rinse step did not have an effect on the purity of carbon dioxide during that step and it was constant for all three runs.

The overall purity of the carbon dioxide increased mainly due to the smaller decay of the component concentration front during the purge step in Run 1. The recovery of carbon dioxide increased at smaller feed to purge ratios, but it was not analyzed in this study, because carbon dioxide is not a valuable product. A part of the carbon dioxide product is used in this study to increase the carbon dioxide purity during the rinse step by using a storage tank at 1 bar in the product end. This performs as a carbon dioxide 'make-up' tank to recycle the carbon dioxide product in the PSA process.

The purge-to-feed flow rate had a greater effect than did both the superficial gas velocity and the bed length on the hydrogen recovery, with overall deviations of about 5% in for the simulated runs. Run 1 also gave the best result for this performance parameter, because less hydrogen was recycled to the purge. The recovery of hydrogen for this run was above 90%, which is in an acceptable range for a NGCC power plant.

4.3. Additional configurations for the scaled-up PSA model

The PSA process shown in Figure 1 obtained a maximum purity of hydrogen of 99.994% and a recovery of 92.27%, varying the scaled-up parameters. The maximum purity obtained for carbon dioxide was 95.37%, which is in the acceptable limit value of 95% purity for carbon dioxide storage and utilization. Additional configurations were tested in order to improve the hydrogen recovery and the purity of carbon dioxide.

4.3.1. Addition of an assisted purge step

The overall purity of the carbon dioxide of the four-bed PSA model decreased mainly due to the light fractions of hydrogen entering the bed during the depressurization step. In order to

increase the overall purity of the carbon dioxide, an assisted purge step was added to the four-bed PSA model. Figure 8 shows the flow chart for the four-bed PSA model with an assisted purge step.

Figure 8.

As shown in this figure, the gas component fractions during the depressurization step go to the purging bed. Therefore, a fraction of hydrogen during the adsorption step is not recycled during a purge step of the process. Instead, the light fractions during the depressurization step are recycled to the process, as carbon dioxide starts desorbing around 1 bar (t = 600 s), as shown in Figure 6. Figure 9 shows the concentration fronts of the products for the four-bed PSA model with an assisted purge.

Figure 9.

In Figure 9, the concentration fronts of the components for the adsorption, depressurization, purge and rinse steps did not change much, compared to those from the four-bed model without an assisted purge. The concentration fronts did change slightly during the 50 s of the purge step and pressurization step due to the components coming from the depressurization step instead of the hydrogen. The purity of the hydrogen remained constant for this configuration, at 99.994%, compared to the purity from the four-bed reference model. However, the recovery of hydrogen increased to 94.35%, due to not using

hydrogen as a feed for the purge step. The hydrogen that was not diverted to the purge formed part of the hydrogen product during the adsorption step. There was a slight increase of the carbon dioxide recovery to a value of 90.56%, due to having a less pure stream of hydrogen in the inlet of the purge step.

The carbon dioxide purity increased to 96.12% due to not obtaining the light component fractions during the depressurization step. This step enables to obtain over 95% purity of carbon dioxide, without the addition of more than four beds. A previous study reported a purity of carbon dioxide of 98% after a PSA and a flash separation, but the separation process included seven fixed-bed reactors (Riboldi et al., 2014).

4.3.2. Addition of pressure equalization steps

Industrial PSA reactors usually have more than one pressure equalization step; this requires additional beds. One and two beds were added to the process mainly to improve the recovery of the light product. A maximum of three pressure equalization steps were included in this work; there would be additional capital costs if there were more than six fixed-bed reactors in a power plant. The total duration of the pressure equalization step was kept constant for the synchronization of the steps. For the five-bed model each of the pressure equalization steps lasted 125 s, and for the six-bed model each of the steps lasted 83.3 s. Table 5 and Table 6 show the configuration of the steps for the five- and six-bed models, with two and three pressure equalization steps, respectively. Figure 10 shows the flow chart for the five-bed PSA model with two pressure equalization steps.

Figure 10.

Table 5. Step configuration for the five-bed PSA model with two pressure equalization steps and an assisted purge step.

Steps	1	2	3	4	5	6	7	8	9	10
Bed 1		A		D1	D2	A-Pu	R	Pu	P1	P2	P
Bed 2	P2		P		A		D1	D2	A-Pu	R	Pu	P1
Bed 3	Pu	P1	P2	P		A		D1	D2	A-Pu	R
Bed 4	A-Pu	R	Pu	P1	P2	P		A		D1	D2
Bed 5	D1	D2	A-Pu		Pu		P1	P2	P		A

Table 6. Step configuration for the six-bed PSA model with three pressure equalization steps and an assisted purge step.

Steps	1	2	3	4	5	6	7	8	9	10	11	12
Bed 1		A		D1	D2	D3	A-Pu	R	Pu	P1	P2	P3	P
Bed 2	P3		P		A		D1	D2	D3	A-Pu	R	Pu	P1	P2
Bed 3	P1	P2	P3	P		A		D1	D2	D3	A-Pu	R	Pu
Bed 4	R	Pu	P1	P2	P3	P		A		D1	D2	D3	A-Pu
Bed 5	D3	A-Pu	R	Pu	P1	P2	P3	P		A		D1	D2
Bed 6	D1	D2	D3	A-Pu	R	Pu	P1	P2	P3	P		A

The first pressure equalization-depressurization step (D1) had the lightest fractions of all the pressure equalization steps. This step was used in the third pressure equalization-pressurization step to clean the bed for the six-bed model, based on the component fractions profile in the outlet of the reactor for the four-bed model. Because the assisted purge step was also used for the five- and six-bed models, the purity of carbon dioxide was expected to be over 95%, with the previously mentioned requirement of over 90% hydrogen recovery. Table 7 shows the product performance parameters for the stated bed configurations when varying the number of pressure equalization steps.

571 **Table 7.** PSA product performance indicator values and variable values for a number of bed
572 configurations using an assisted purge step.

Number of beds	Number of PEs	Recovery H_2 (%)	Recovery CO_2 (%)	Purity H_2 (%)	Purity CO_2 (%)
4	1	94.35	90.56	99.994	96.12
5	2	95.61	90.42	99.994	97.18
6	3	96.87	90.37	99.994	97.39

573

574 Table 7 shows that although the purity of hydrogen remained constant over a varying
575 number of pressure equalization steps, the recovery of this component increased by more than
576 2 percentage points from a four-bed to a six-bed PSA model. There was a slight decrease of
577 the recovery of the carbon dioxide to a value of 90.37% with three pressure equalization steps.
578 The purity of carbon dioxide increased by 1 percentage point from the four- to the five-bed
579 model. However, it increased by only 0.2 from the five- to the six-bed model. Previous work
580 has not reported the effect of pressure equalization steps in the carbon dioxide purity, but
581 showed to increase the recovery of the hydrogen product by two percentage points (Luberti et
582 al., 2014).

583

584 *4.3.3. Addition of a rinse step after the feed or pressure equalization steps*

585 The effect on the PSA performance parameters of adding a rinse step after the feed step was
586 investigated for the four-bed PSA model and across the various pressure equalization steps for
587 the five- and six-bed models. This step was studied after the feed and after each step of the
588 pressure equalization steps. For the five-bed model, the rinse was applied after the first pressure
589 equalization step (D1) and, after the second pressure equalization step (D2) for the six-bed PSA
590 model. Table 8 shows the product performance parameters for a number of configurations
591 using the rinse step.

592

593 **Table 8.** Product performance indicator values and variable values for a number of bed
594 configurations using the assisted purge step and the rinse step.

Number of beds	Number of PEs	Rinse position	Recovery H_2 (%)	Recovery CO_2 (%)	Purity H_2 (%)	Purity CO_2 (%)
4	1	A-PE1	95.48	90.76	99.991	98.28
5	2	PE1-PE2	96.07	90.57	99.994	98.56
6	3	PE2-PE3	97.02	90.49	99.994	98.74

595

596 As shown in Table 8, the purity of hydrogen decreased insignificantly by 0.003 percentage
597 points in the four-bed PSA model with a rinse step after the feed step (A-PE1) compared to the
598 model without this step. The small decrease was due to the rinse that the carbon dioxide feed
599 adsorbed inside the reactor at 37.6 bar. This is further clarified in Figure 11, where the carbon
600 dioxide did not come out of the bed until it finished the depressurization step. The recovery of
601 hydrogen did slightly increase by 1 percentage point due to not feeding gas during the rinse
602 step and still obtain hydrogen. The recovery of carbon dioxide also increased slightly, due to
603 recycling the carbon dioxide at high pressures, and then obtaining the product at atmospheric
604 pressures. The purity of carbon dioxide increased between 1 and 2 percentage points when
605 adding the rinse step to the various PSA configurations with pressure equalization.

606

607 **Figure 11**

608

609 The effect of the rinse step at pressures higher than 1 bar has not been previously reported
610 to pressure swing adsorption processes applied to hydrogen purification and carbon capture in
611 IGCC power plants (Luberti et al., 2014; Moon et al., 2018; Ribeiro et al., 2008; Riboldi et al.,
612 2014). A similar step has been previously reported where the outlet gas of the purge step is

recycled to the adsorption step to obtain a carbon dioxide purity over 95% (Wang et al., 2015). This step also shows an improvement on the overall hydrogen recovery due to the lower amount of hydrogen fed into the adsorption step when the carbon dioxide is recycled to pressures higher than 1 bar.

5. Conclusions

A laboratory four-bed and seven step PSA model was scaled up to operate in a NGCC power plant and results from the laboratory and scaled-up models were compared. Both processes yielded the same purity and recovery values of 99.999% and 87.6% for the hydrogen, respectively. The carbon dioxide yielded a purity of 86.4% in the scaled-up model, 2% higher than the laboratory model, and a recovery lower than 85% for both cases. The four-bed model PSA included a rinse step at 1 bar which proved to be essential to increase the carbon dioxide purity.

The effects of the parameters in the scaled-up model, such as the bed diameter bed length and purge-to-feed flow rate ratio were investigated by using global system analysis (GSA) to maximize the product performance parameters. At high velocities, such as 0.048 m s^{-1}, and at a bed diameter of 2.38 m, a carbon dioxide purity of 92.93% was obtained. This can be explained by the increase of the mass transfer between the gas and the solid phase. The carbon dioxide purity increased further to 95.37% with a bed length of 4 m and a purge-to-feed flow rate ratio of 0.22. The purity of hydrogen remained nearly constant with a value of 99.99% for all the GSA cases. The recovery of hydrogen decreased to 84.56% at gas velocities of 0.048 m s^{-1}, but it increased further at purge-to-feed flow rate ratios of 0.22 to 92.27%. The recovery of carbon dioxide yielded a value of 90.11% in this case.

636 Additional PSA configurations were studied to improve the carbon dioxide purity and the
637 hydrogen recovery. These configurations included an assisted purge step, which increased the
638 hydrogen recovery to 94.35%. This assisted purge step also proved to be essential to obtain
639 carbon dioxide purities over 96%. These purities increased slightly (by 1 percentage point)
640 upon the introduction of two (five-bed model) and three (six-bed model) pressure equalization
641 steps. The main performance parameter which increased with the number of pressure
642 equalization steps was the hydrogen recovery by 2 percentage points, by including three
643 pressure equalization steps. The recovery of carbon dioxide varied less than 1 percentage point
644 with the introduction of pressure equalization steps.

645 The number of pressure equalization steps increases with the number of beds, which
646 increases the CAPEX of the plant. The use of a rinse step after the feed or pressure equalization
647 step increased the carbon dioxide purity by around 2% percentage points, obtaining a maximum
648 of 98.74% purity for the six-bed model. This model included the rinse step after a second
649 pressure equalization step. A compressor is required for this rinse step, which also affects the
650 CAPEX of the plant.

651 Overall, the four-bed model with an assisted purge step and a rinse step higher than 1 bar
652 showed promising results, due to the lower capital costs expected for a power plant with
653 decreasing number of fixed-bed units, and based on the cyclic capacity required to operate the
654 gas turbine. The CAPEX and the OPEX of the designed PSA process integrated with a NGCC
655 power plant will be studied in the near future.

656

657 **Acknowledgements**

658 This work was supported financially by the EPSRC and the Centre for Doctoral Training in
659 Carbon Capture and Storage and Cleaner Fossil Energy (EP/L016362/1). gPROMS®
660 ProcessBuilder software was provided in-kind by Process Systems Enterprise (PSE).

References

Abanades, J.C., Arias, B., Lyngfelt, A., Mattisson, T., Wiley, D.E., Li, H., Ho, M.T., Mangano, E., Brandani, S., 2015. Emerging CO_2 capture systems. Int. J. Greenh. Gas Control 40, 126–166. https://doi.org/10.1016/j.ijggc.2015.04.018

Agarwal, A., Biegler, L.T., Zitney, S.E., 2010. Superstructure-based optimal synthesis of pressure swing adsorption cycles for precombustion CO_2 capture. Ind. Eng. Chem. Res. 49, 5066–5079. https://doi.org/10.1021/ie900873j

Azpiri Solares, R.A., Soares dos Santos, D., Ingram, A., Wood, J., 2019. Modelling and parameter estimation of breakthrough curves for amine-modified activated carbons under pre-combustion carbon capture conditions. Fuel 253, 1130–1139. https://doi.org/10.1016/j.fuel.2019.05.095

Budinis, S., Krevor, S., Dowell, N. Mac, Brandon, N., Hawkes, A., 2018. An assessment of CCS costs, barriers and potential. Energy Strateg. Rev. 22, 61–81. https://doi.org/10.1016/j.esr.2018.08.003

Cappelletti, A., Martelli, F., 2017. Investigation of a pure hydrogen fueled gas turbine burner. Int. J. Hydrogen Energy 42, 10513–10523. https://doi.org/10.1016/j.ijhydene.2017.02.104

Casas, N., Schell, J., Joss, L., Mazzotti, M., 2013. A parametric study of a PSA process for pre-combustion CO_2 capture. Sep. Purif. Technol. 104, 183–192. https://doi.org/10.1016/j.seppur.2012.11.018

Cavenati, S., Grande, C.A., Rodrigues, A.E., 2006. Separation of $CH_4/CO_2/N_2$ mixtures by layered pressure swing adsorption for upgrade of natural gas. Chem. Eng. Sci. 61, 3893–3906. https://doi.org/10.1016/j.ces.2006.01.023

European Benchmarking Task Force, 2011. European best practice guidelines for assessment of CO_2 capture technologies. Enabling Advanced Pre-combustion Capture Tecniques and Plants. D 1.4.3

Gasworld, 2019. Carbon capture: In focus like never before, but are we doing enough? https://www.gasworld.com/carbon-capture-in-focus-like-never-before-but-are-we-doing-enough/2017994.article (accessed 26 November 2019)

Goldmeer, J., 2018. Fuel Flexible Gas Turbines as Enablers for a Low or Reduced Carbon Energy Ecosystem. GE, Electrify Eur. https://www.ge.com/content/dam/gepower/global/en_US/documents/fuel-flexibility/GEA33861%20-%20Fuel%20Flexible%20Gas%20Turbines%20as%20Enablers%20for%20a%20Low%

20Carbon%20Energy%20Ecosystem.pdf (accessed 9 June 2019)

Grande, C.A., 2012. Advances in Pressure Swing Adsorption for Gas Separation. ISRN Chem. Eng. 2012, 1–13. https://doi.org/10.5402/2012/982934

Grande, C.A., Roussanaly, S., Anantharaman, R., Lindqvist, K., Singh, P., Kemper, J., 2017. CO_2 Capture in Natural Gas Production by Adsorption Processes, in: Energy Procedia. https://doi.org/10.1016/j.egypro.2017.03.1363

Heuberger, C.F., Staffell, I., Shah, N., MacDowell, N., 2017. What is the Value of CCS in the Future Energy System? Energy Procedia 114, 7564–7572. https://doi.org/10.1016/j.egypro.2017.03.1888

Jain, S., Moharir, A.S., Li, P., Wozny, G., 2003. Heuristic design of pressure swing adsorption: A preliminary study. Sep. Purif. Technol. 33, 25–43. https://doi.org/10.1016/S1383-5866(02)00208-3

Jansen, D., Gazzani, M., Manzolini, G., Dijk, E. Van, Carbo, M., 2015. Pre-combustion CO_2 capture. Int. J. Greenh. Gas Control 40, 167–187. https://doi.org/10.1016/j.ijggc.2015.05.028

Jiang, L., Fox, V.G., Biegler, L.T., 2004. Simulation and optimal design of multiple-bed pressure swing adsorption systems. AIChE J. 50, 2904–2917. https://doi.org/10.1002/aic.10223

Ju, Y., Lee, C.H., 2017. Evaluation of the energy efficiency of the shell coal gasification process by coal type. Energy Convers. Manag. 143, 123–136. https://doi.org/10.1016/j.enconman.2017.03.082

Lee, H.H., Lee, J.C., Joo, Y.J., Oh, M., Lee, C.H., 2014. Dynamic modeling of Shell entrained flow gasifier in an integrated gasification combined cycle process. Appl. Energy 131, 425–440. https://doi.org/10.1016/j.apenergy.2014.06.044

Lee, J.C., Lee, H.H., Joo, Y.J., Lee, C.H., Oh, M., 2014. Process simulation and thermodynamic analysis of an IGCC (Integrated Gasification Combined Cycle) plant with an entrained coal gasifier. Energy 64, 58–68.

Lee, W.S., Lee, J.C., Oh, H.T., Baek, S.W., Oh, M., Lee, C.H., 2017. Performance, economic and exergy analyses of carbon capture processes for a 300 MW class integrated gasification combined cycle power plant. Energy 134, 731–742. https://doi.org/10.1016/j.energy.2017.06.059

Luberti, M., Friedrich, D., Brandani, S., Ahn, H., 2014. Design of a H_2 PSA for cogeneration of ultrapure hydrogen and power at an advanced integrated gasification combined cycle with pre-combustion capture. Adsorption 20, 511–524. https://doi.org/10.1007/s10450-013-9598-0

Mac Dowell, N., Staffell, I., 2016. The role of flexible CCS in the UK's future energy system. Int. J. Greenh. Gas Control 48, 327–344. https://doi.org/10.1016/j.ijggc.2016.01.043

Moon, D.K., Lee, D.G., Lee, C.H., 2016. H_2 pressure swing adsorption for high pressure syngas from an integrated gasification combined cycle with a carbon capture process. Appl. Energy 183, 760–774. https://doi.org/10.1016/j.apenergy.2016.09.038

Moon, D.K., Park, Y., Oh, H.T., Kim, S.H., Oh, M., Lee, C.H., 2018. Performance analysis

of an eight-layered bed PSA process for H_2 recovery from IGCC with pre-combustion carbon capture. Energy Convers. Manag. 156, 202–214. https://doi.org/10.1016/j.enconman.2017.11.013

Nikolic, D., Giovanoglou, A., Georgiadis, M.C., Kikkinides, E.S., 2008. Generic modeling framework for gas separations using multibed pressure swing adsorption processes. Ind. Eng. Chem. Res. 47, 3156–3169. https://doi.org/10.1021/ie0712582

Rackley, S.A., 2017. Carbon Capture and Storage (2nd ed). Elsevier, 73–102. https://doi.org/10.1016/B978-0-12-812041-5.00004-0

Rase, H.F., 1990. Fixed-Bed Reactor Design and Diagnostics (1st ed). Elsevier. https://doi.org/10.1016/c2013-0-04268-5

Ribeiro, A.M., Grande, C.A., Lopes, F.V.S., Loureiro, J.M., Rodrigues, A.E., 2008. A parametric study of layered bed PSA for hydrogen purification. Chem. Eng. Sci. 63, 5258–5273. https://doi.org/10.1016/j.ces.2008.07.017

Riboldi, L., Bolland, O., 2016. Pressure swing adsorption for coproduction of power and ultrapure H_2 in an IGCC plant with CO_2 capture. Int. J. Hydrogen Energy 41, 10646–10660. https://doi.org/10.1016/j.ijhydene.2016.04.089

Riboldi, L., Bolland, O., 2015a. Evaluating Pressure Swing Adsorption as a CO_2 separation technique in coal-fired power plants. Int. J. Greenh. Gas Control 39, 1–16. https://doi.org/10.1016/j.ijggc.2015.02.001

Riboldi, L., Bolland, O., 2015b. Comprehensive analysis on the performance of an IGCC plant with a PSA process integrated for CO_2 capture. Int. J. Greenh. Gas Control 43, 57–69. https://doi.org/10.1016/j.ijggc.2015.10.006

Riboldi, L., Bolland, O., Ngoy, J.M., Wagner, N., 2014. Full-plant analysis of a PSA CO_2 capture unit integrated in coalfired power plants: Post- And pre-combustion scenarios. Energy Procedia 63, 2289–2304. https://doi.org/10.1016/j.egypro.2014.11.248

Ruthven, D.M., Douglas, M., Farooq, S., Knaebel, K.S., 1994. Pressure swing adsorption. VCH Publishers. https://doi.org/10.1002/aic.690410122

Seyitoglu, S.S., Dincer, I., Kilicarslan, A., 2016. Assessment of an IGCC based trigeneration system for power, hydrogen and synthesis fuel production. Int. J. Hydrogen Energy 41, 8168–8175. https://doi.org/10.1016/j.ijhydene.2015.10.093

U.S. Energy Information Administration (EIA), 2017. Petra Nova is one of two carbon capture and sequestration power plants in the world. https://www.eia.gov/todayinenergy/detail.php?id=33552 (accessed 11 June 2019)

Wakao, N., Funazkri, T., 1978. Effect of fluid dispersion coefficients on particle-to-fluid mass transfer coefficients in packed beds. Correlation of sherwood numbers. Chem. Eng. Sci. 33, 1375–1384. https://doi.org/10.1016/0009-2509(78)85120-3

Wang, Y., Dowling, A.W., Krieft, C., Walther, A., Biegler, L.T., 2015. Pressure Swing Adsorption Optimization Strategies for CO_2 Capture, Computer Aided Chemical Engineering. https://doi.org/10.1016/B978-0-444-63472-6.00008-2

Webley, P.A., 2014. Adsorption technology for CO_2 separation and capture: A perspective. Adsorption 20, 225–231. https://doi.org/10.1007/s10450-014-9603-2

Wiheeb, A.D., Helwani, Z., Kim, J., Othman, M.R., 2016. Pressure Swing Adsorption Technologies for Carbon Dioxide Capture. Sep. Purif. Rev. 45, 108–121. https://doi.org/10.1080/15422119.2015.1047958

List of Figure Captions

Figure 1. Schematic figure of the seven-step four-bed PSA model.

Figure 2. Flow diagram of the PSA parameters studied using GSA.

Figure 3a. Component concentration profiles at the end of the bed for the seven-step four-bed PSA model at laboratory scale.

Figure 3b. Component concentration profiles at the end of the bed for the seven-step four-bed PSA scaled-up model.

Figure 4. Evolution of the gas phase temperature at the end of the fixed-bed reactor for the four-bed scaled-up process.

Figure 5. Carbon dioxide purity results for the GSA analysis varying the superficial velocity.

Figure 6. Carbon dioxide concentration profiles at the end of the bed for a number of bed length-to-diameter ratios.

Figure 7. Carbon dioxide purity results for the GSA analysis varying the purge-to-feed flow rate ratio.

Figure 8. Schematic figure of the four-bed PSA model, adding an assisted purge step.

Figure 9. Component concentration profiles at the end of the bed for the four-bed PSA model adding an assisted purge step.

Figure 10. Schematic figure of the five-bed PSA model with two pressure equalization steps.

Figure 11. Component concentration profiles at the end of the bed for the four-bed PSA model adding a rinse step.

Figure 1

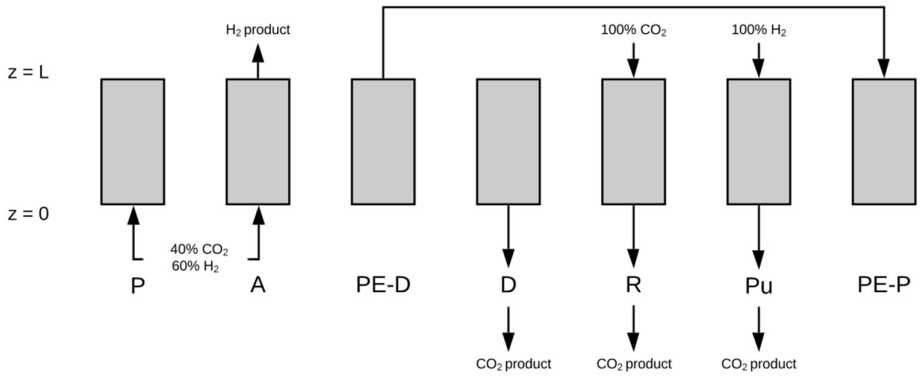
z = L
z = 0
H2 product
100% CO2
100% H2
40% CO2
60% H2
P
A
PE-D
D
R
Pu
PE-P
CO2 product
CO2 product
CO2 product

Figure 2

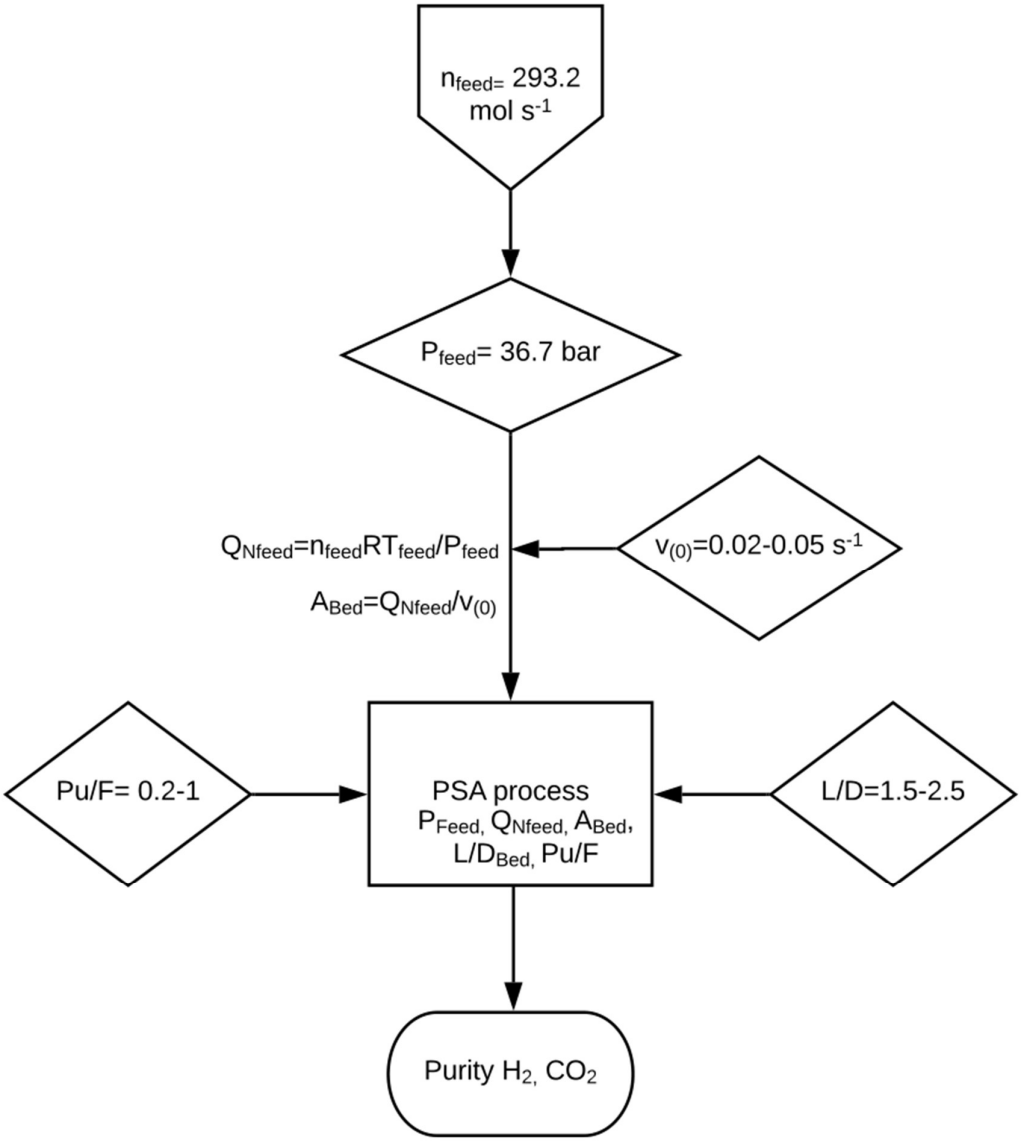
$n_{feed=}$ 293.2 mol s^{-1}
P_{feed}= 36.7 bar
$Q_{Nfeed}=n_{feed}RT_{feed}/P_{feed}$
$A_{Bed}=Q_{Nfeed}/v_{(0)}$
$v_{(0)}$=0.02-0.05 s^{-1}
Pu/F= 0.2-1
PSA process
P_{Feed}, Q_{Nfeed}, A_{Bed}, L/D_{Bed}, Pu/F
L/D=1.5-2.5
Purity H_2, CO_2

Figure 3a

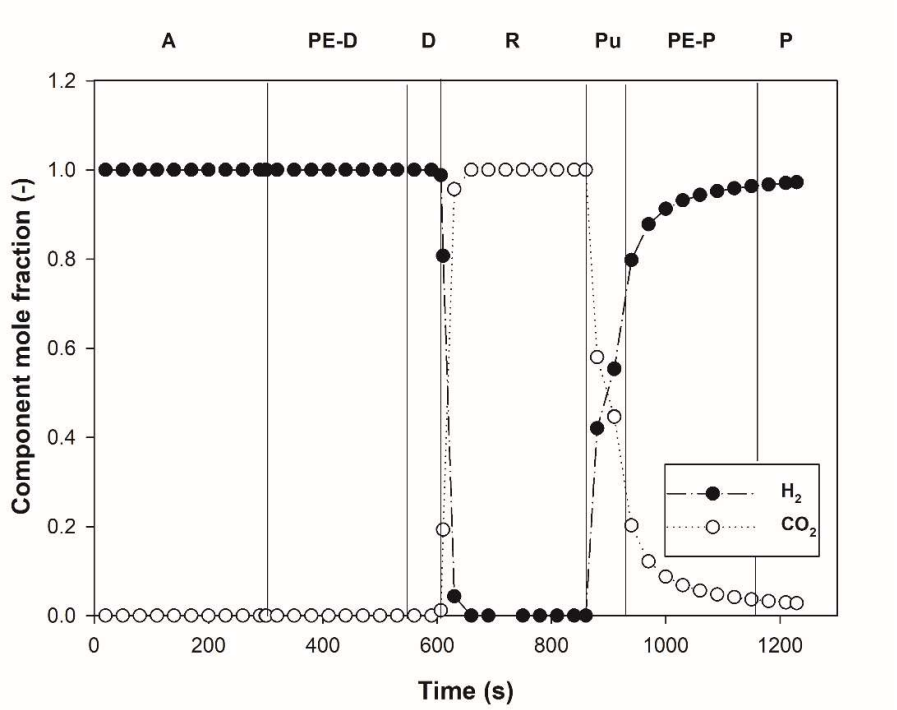

Figure 3b

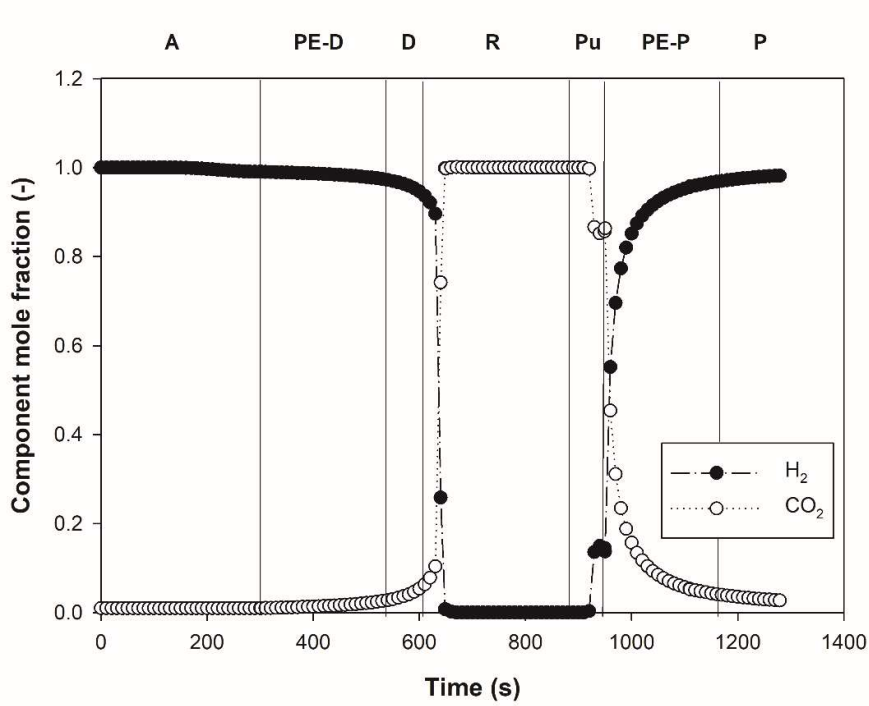

Figure 4

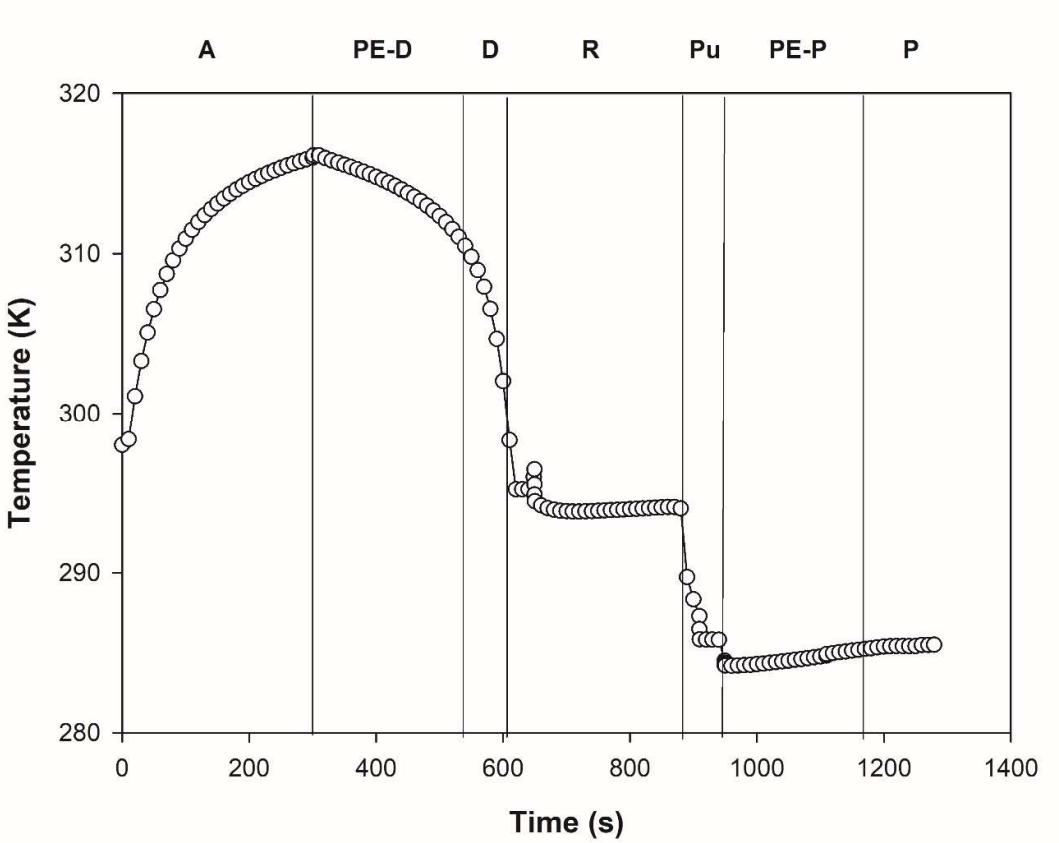
A
PE-D
D
R
Pu
PE-P
P
320
310
300
290
280
Temperature (K)
0
200
400
600
800
1000
1200
1400
Time (s)

Figure 5

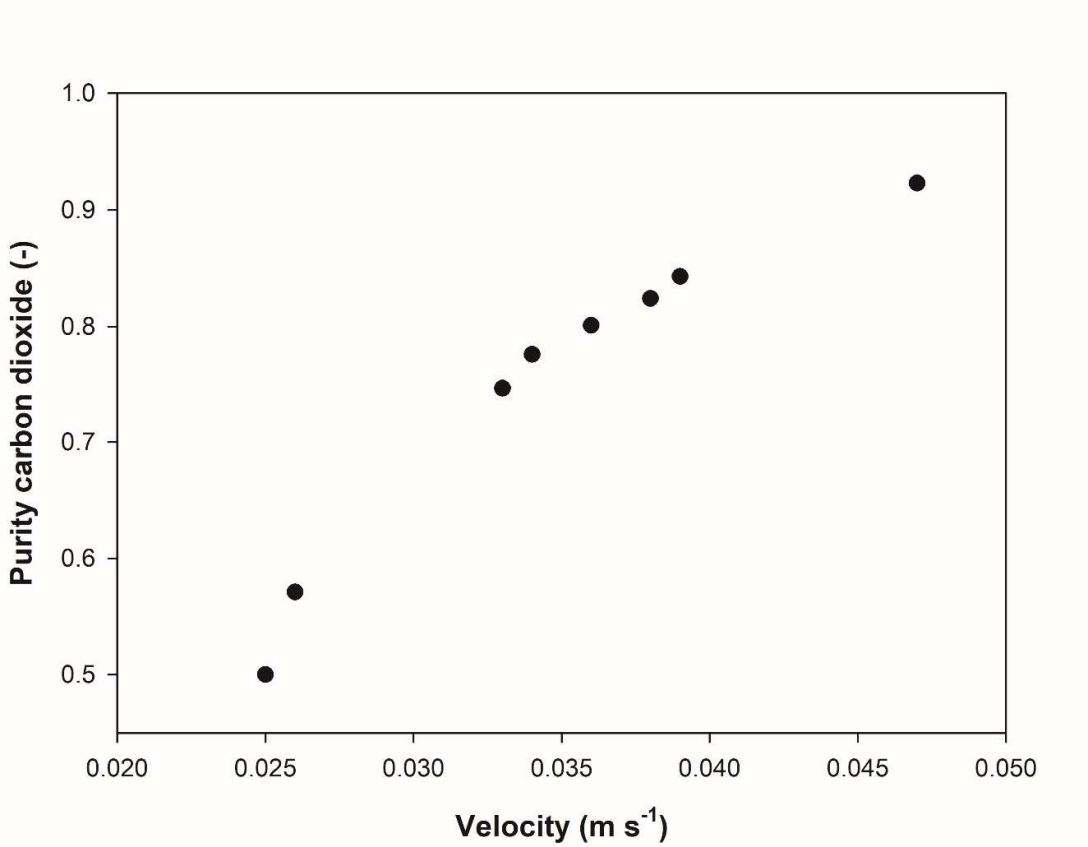
Purity carbon dioxide (-)
1.0
0.9
0.8
0.7
0.6
0.5
0.020
0.025
0.030
0.035
0.040
0.045
0.050
Velocity (m s-1)

Figure 6

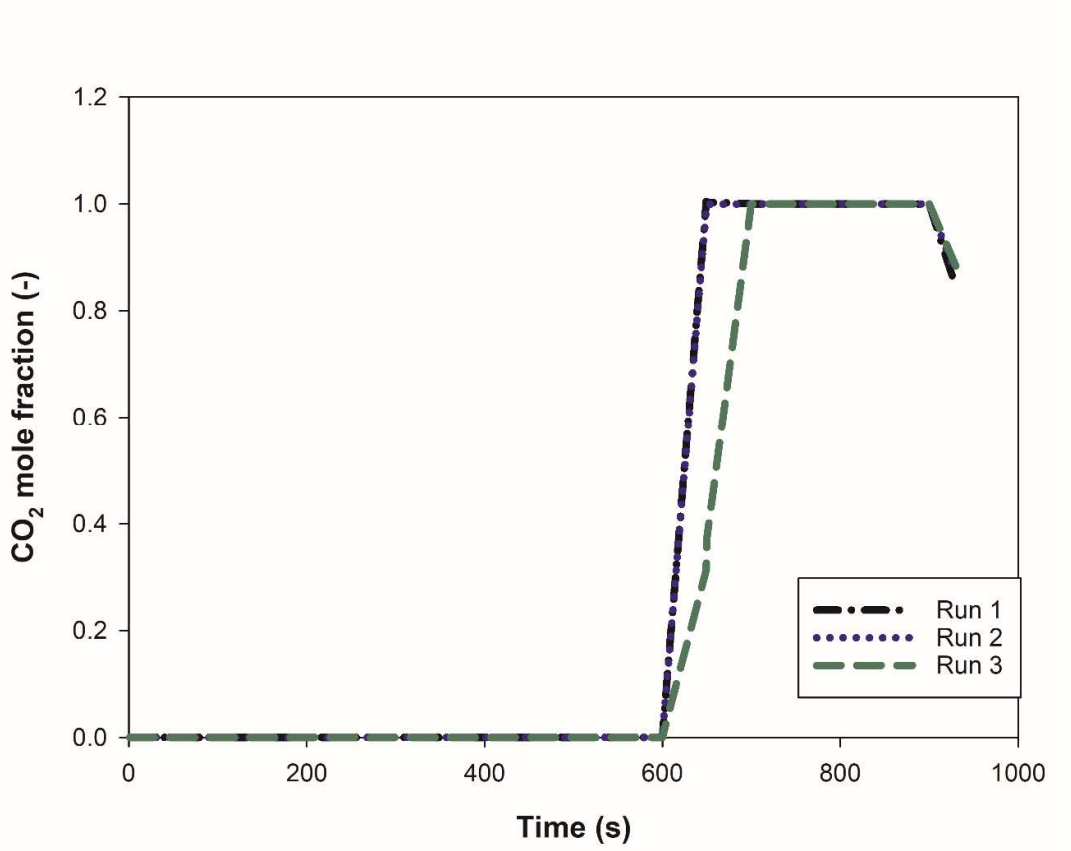
1.2
1.0
0.8
0.6
0.4
0.2
0.0
CO_2 mole fraction (-)
0
200
400
600
800
1000
Time (s)
Run 1
Run 2
Run 3

Figure 7

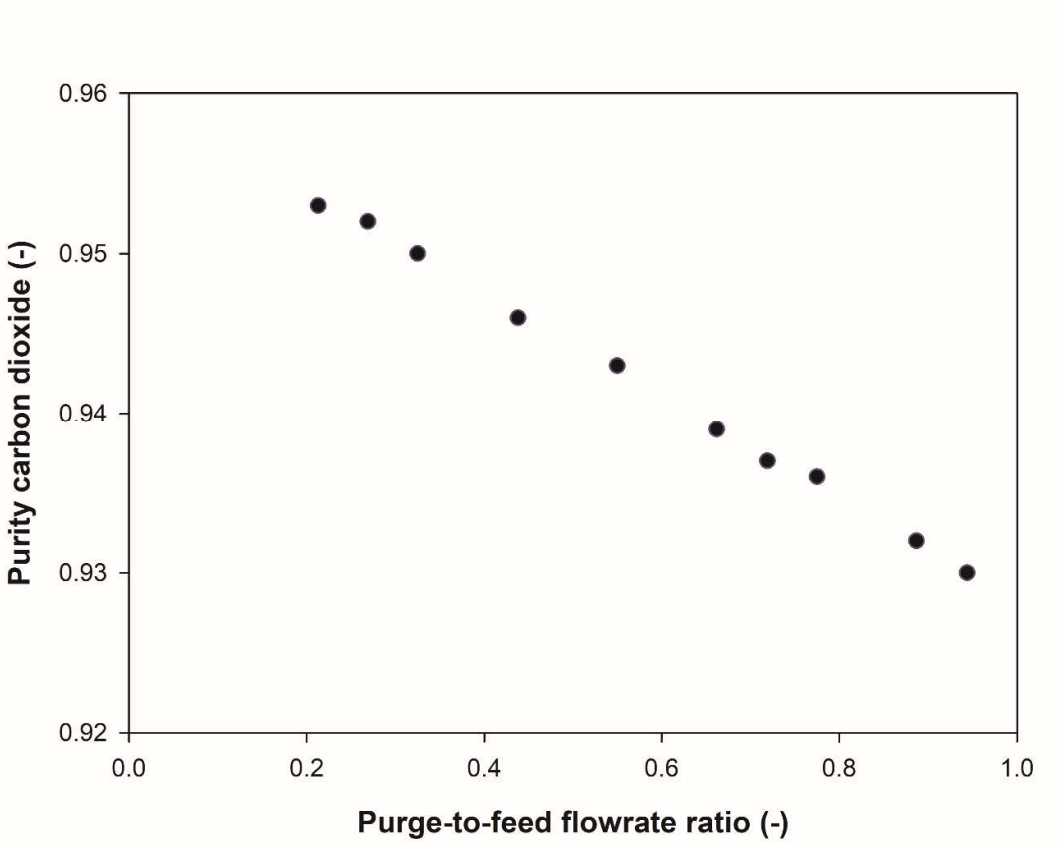
0.96
0.95
0.94
0.93
0.92
Purity carbon dioxide (-)
0.0
0.2
0.4
0.6
0.8
1.0
Purge-to-feed flowrate ratio (-)

Figure 8

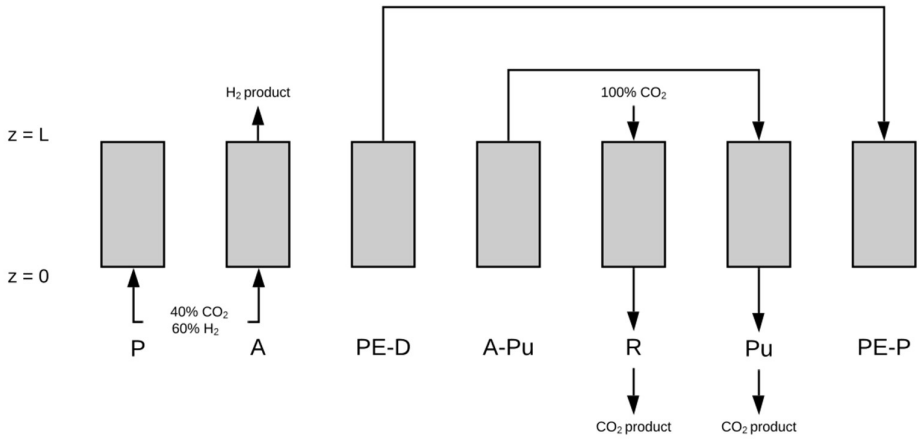
z = L
z = 0
H2 product
100% CO2
40% CO2
60% H2
P
A
PE-D
A-Pu
R
Pu
PE-P
CO2 product
CO2 product

Figure 9

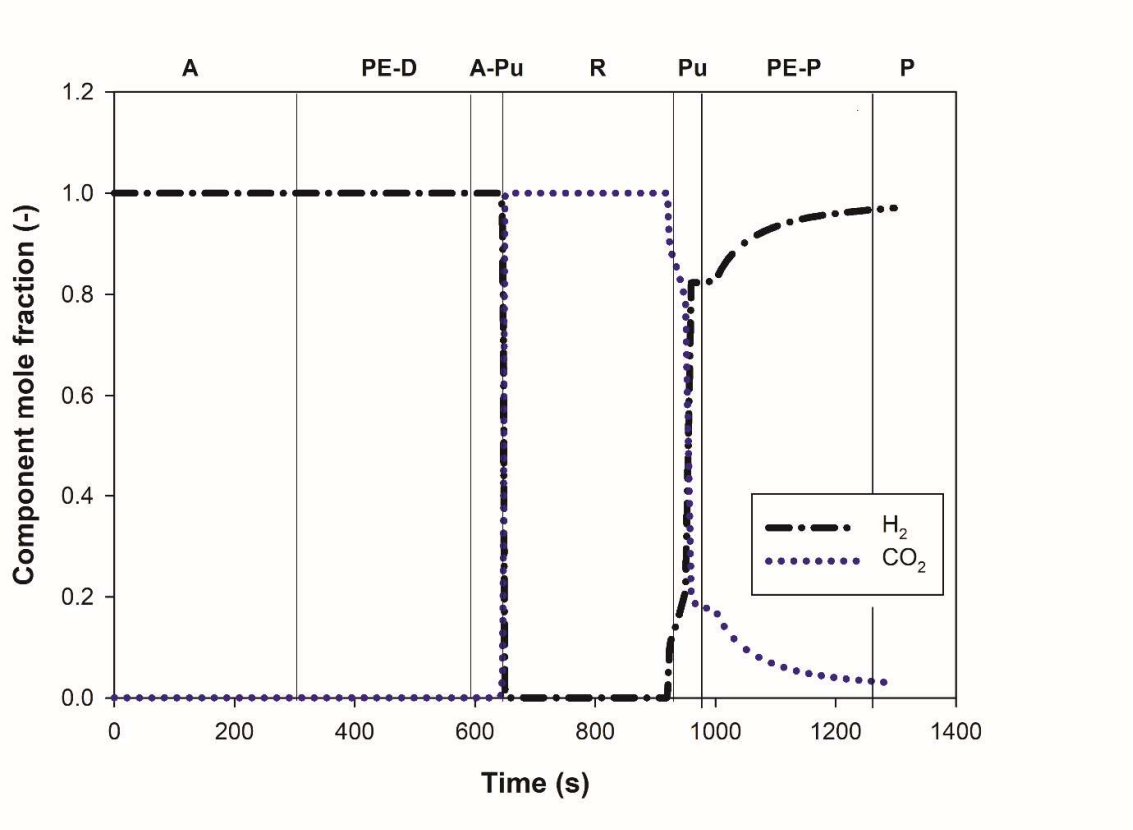
A
PE-D
A-Pu
R
Pu
PE-P
P
1.2
1.0
0.8
0.6
0.4
0.2
0.0
Component mole fraction (-)
0
200
400
600
800
1000
1200
1400
Time (s)
H2
CO2

Figure 10

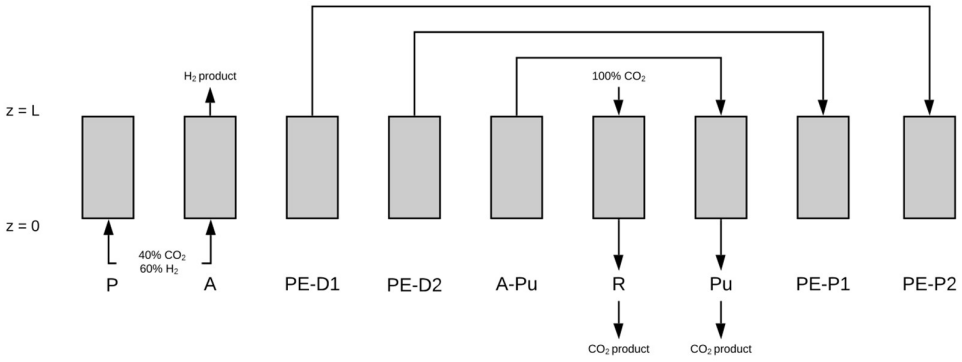
z = L
z = 0
H2 product
100% CO2
40% CO2
60% H2
P
A
PE-D1
PE-D2
A-Pu
R
Pu
PE-P1
PE-P2
CO2 product
CO2 product

Figure 11

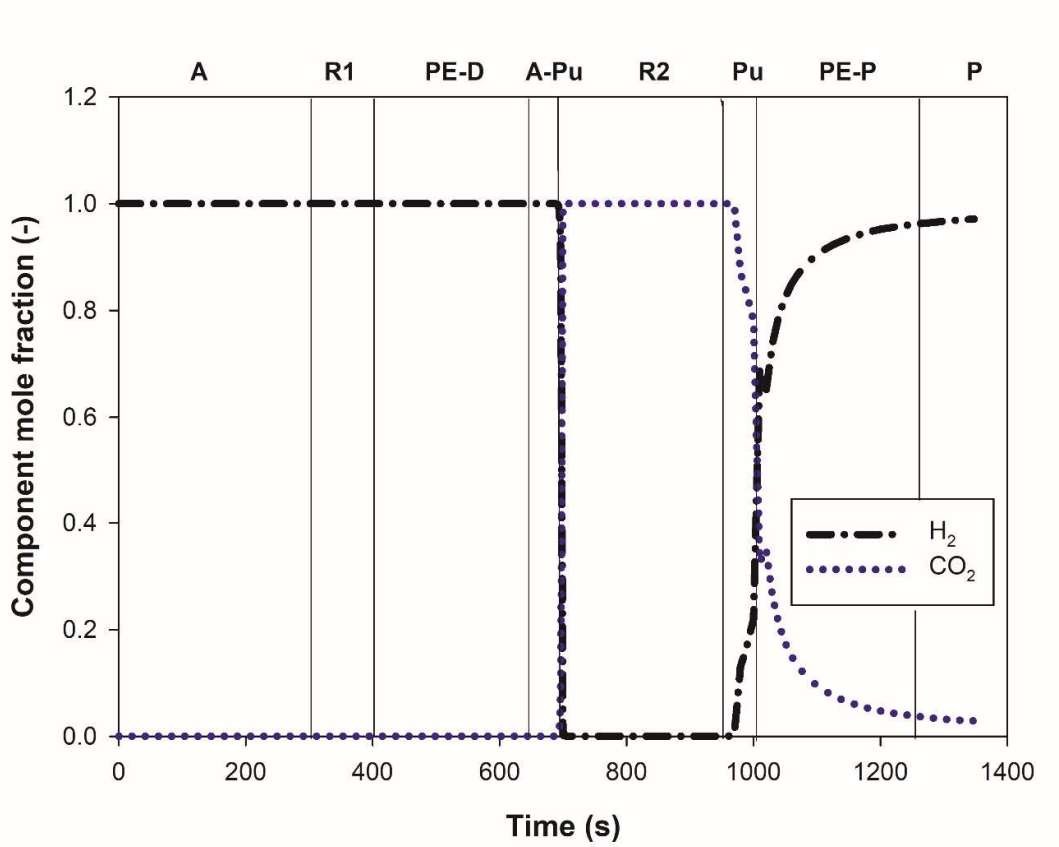
A
R1
PE-D
A-Pu
R2
Pu
PE-P
P
1.2
1.0
0.8
0.6
0.4
0.2
0.0
Component mole fraction (-)
0
200
400
600
800
1000
1200
1400
Time (s)
H2
CO2

Graphical Abstract